Humanized Radioiodinated Minibody For Imaging of Prostate Stem Cell Antigen – Expressing Tumors

Jeffrey V. Leyton,[1] Tove Olafsen,[1] Eric J. Lepin,[1] Scott Hahm,[2] Karl B. Bauer,[1] Robert E. Reiter,[2] and Anna M. Wu[1]

Abstract

Purpose: Prostate stem cell antigen (PSCA) is a cell surface glycoprotein that is overexpressed in prostate cancer, including hormone refractory disease. Previous preclinical studies showed the intact anti-PSCA antibodies, 1G8 and hu1G8, localized specifically to PSCA-expressing xenografts. Optimal micro positron emission tomography (microPET) imaging using hu1G8, however, required a delay of 168 hours postinjection. In this study, the 2B3 minibody (an 80-kDa engineered antibody fragment) has been produced for rapid targeting and imaging.

Experimental Design: A gene encoding a PSCA-specific minibody, V_L-linker-V_H-hinge-huIgG1 C_H3, was assembled. The minibody was expressed by secretion from mammalian cells and purified by cation exchange chromatography. Relative affinity and specificity were determined by competition ELISA and flow cytometry. Serial microPET imaging using a ^{124}I-labeled minibody was conducted at 4 and 21 hours in mice bearing LAPC-9 AD, LAPC-9 AI, PC-3, and LNCaP-PSCA human prostate cancer xenografts. Tumor and tissue biodistribution was determined, and region of interest analysis of the images was conducted.

Results: Yields of 20 mg/L purified 2B3 minibody were obtained that showed specific binding to LNCaP-PSCA cells. Purified 2B3 minibody showed specific binding to LNCaP-PSCA cells with an apparent affinity of 46 nmol/L. Radioiodinated 2B3 minibody showed rapid nontarget tissue and blood clearance kinetics ($t_{1/2}\beta$ = 11.2 hours). MicroPET scanning using the ^{124}I-2B3 minibody showed both androgen-dependent and -independent tumors as early as 4 hours and excellent high contrast images at 21 hours postinjection.

Conclusions: Imaging PSCA-positive prostate cancer is feasible using an intermediate size antibody fragment at 21 hours.

Prostate cancer is the most commonly diagnosed and second leading cause of cancer related deaths in American men, according to the American Cancer Society. When diagnosed early, the relative 5-year survival rate is 100%. Once a patient has been diagnosed with prostate cancer, appropriate staging and follow-up are required to select the most effective treatment. There are few means of detecting extraprostatic sites of disease or recurrence, and an imaging agent to address these specific needs would contribute to patient management.

Several positron emission tomography (PET) ^{11}C- and ^{18}F-based radiotracers including ^{18}F-fluorodeoxyglucose have been developed and evaluated for imaging of prostate cancer (1–4). However, ^{11}C-based radiotracers are impractical without an onsite cyclotron and ^{18}F-labeled small molecule tracers generally exhibit high urinary excretion. In addition, factors such as nonspecific uptake, low glucose utilization, and inefficient radiolabeling and synthesis methods have made it difficult to fully implement various radiotracers into the clinic (5). A recent pilot clinical study using the anti-1-amino-3-^{18}F-fluorocyclobutane-1-carboxylic acid (anti-^{18}F-FACBC) synthetic L-leucine analogue has shown promise in imaging prostate cancer (6). The anti-^{18}F-FACBC showed localization to primary, metastatic, and recurrent prostate carcinoma with variable but relatively low renal excretion and bladder activity. However, this tracer shared some of the characteristics often observed with metabolic tracers, such as nonspecific uptake—in this case, incidental bowel uptake, occasional low-level uptake in benign inguinal lymph nodes, and regions of false positivity within the prostate.

An approach to overcome nonspecific uptake and false positivity is to develop PET probes that can specifically target tumor cell surface antigens. High expression of receptors on cancer cells compared with normal tissues provides the

Authors' Affiliations: [1]Crump Institute for Molecular Imaging, Department of Molecular and Medical Pharmacology, David Geffen School of Medicine and [2]Department of Urology, University of California at Los Angeles, Los Angeles, California

Received 12/10/07; revised 5/16/08; accepted 5/27/08.

Grant support: University of California at Los Angeles (UCLA) Specialized Programs of Research Excellence in Prostate Cancer grant NIH CA 92131 and a career development award from the UCLA In Vivo Centers for Molecular Imaging of Cancer (NIH grant CA 86306). Additional support by NIH grant P01 CA 43904. R.E. Reiter and A.M. Wu are members of the Jonsson Comprehensive Cancer Center at UCLA (NIH grant CA 16042).

The costs of publication of this article were defrayed in part by the payment of page charges. This article must therefore be hereby marked *advertisement* in accordance with 18 U.S.C. Section 1734 solely to indicate this fact.

Requests for reprints: Anna M. Wu, Crump Institute for Molecular Imaging, Department of Molecular and Medical Pharmacology, David Geffen School of Medicine at University of California at Los Angeles, 700 Westwood Plaza, Box 951770, Los Angeles, CA 90095. Phone: 310-794-5088; E-mail: awu@mednet.ucla.edu.

doi:10.1158/1078-0432.CCR-07-5093

molecular basis for using radiolabeled antigen-specific antibodies to visualize tumors. In prostate cancer, the ^{111}In-labeled monoclonal antibody capromab pendetide (Prostascint; Cytogen Corp.), specific for prostate-specific membrane antigen, has been extensively evaluated clinically and is primarily used for detecting advanced, recurrent local disease and lymph node metastases (7). However, the clinical utility of capromab pendetide is still highly debated due to a low sensitivity (62-75%) caused by slow tumor uptake and poor clearance (8). In addition, capromab pendetide recognizes an internal epitope on prostate-specific membrane antigen (9), which may limit its utility in detecting viable cells. It also suffers from the general limitations of other radiolabeled intact antibodies; despite the ability to effectively deliver high activities to tumors, high background activity in the blood requires delays in imaging for optimal tumor evaluation. Furthermore, repeated administration is precluded due to the murine nature of the antibody.

Another prostate-specific surface marker that is highly suitable for antibody-based therapy and imaging is the prostate stem cell antigen (PSCA), a cysteine-rich 123-aa glycosylphosphatidylinositol-anchored surface glycoprotein (10–12). We have shown in human prostate cancer specimens that >80% of local disease and all metastatic bone lesions examined express PSCA (11). Elevated PSCA expression correlates with increased tumor stage, grade, and progression to androgen independence (11). Moreover, PSCA up-regulation has been detected in bladder and pancreatic cancers (13–15). The restricted PSCA expression in normal tissues makes PSCA an enticing target for immunoimaging and immunotherapy of cancerous lesions.

The murine 1G8 monoclonal antibody, raised against an extracellular epitope of PSCA, has shown antitumor growth properties (16). Targeting, imaging, and therapy using a humanized version of the 1G8 monoclonal antibody (hu1G8) has also been examined in preclinical models (17). Hu1G8 exhibited significant inhibition of tumor take of low PSCA-expressing bladder carcinoma cells. When the antibody was evaluated by PET in LAPC-9-xenografted mice following radioiodination with the positron emitter ^{124}I ($t_{1/2}$ 4.2 d), high contrast images were achieved. However, due to the slow clearance kinetics of this intact humanized antibody, enhanced target-to-background images were not obtained until one week after administration of ^{124}I-hu1G8.

Protein engineering techniques can be used to produce antibody fragments of various sizes, facilitating rapid clearance from the blood. These fragments show improved pharmacokinetics suitable for imaging while maintaining excellent tumor uptake, resulting in high tumor-to-background ratios at early time points (18–20). Tumor targeting with bivalent minibody (scFv-C_H3 dimer, 80 kDa) fragments in mice bearing colorectal and breast cancer xenografts targeting carcinoembryonic antigen and HER-2, respectively, has been achieved (21–23). These minibodies exhibited fast blood clearance and rapid tumor targeting that reached maximum uptake at 12 hours (19, 22, 24). The ^{124}I-labeled anti-carcinoembryonic antigen minibody was further evaluated by microPET imaging in mice bearing human colorectal cancer xenografts (21). This minibody provided excellent tumor uptake and high-contrast images at 18 hours.

The goal of this work was to develop and evaluate a minibody with specificity for PSCA for imaging prostate cancer xenograft–bearing mice. This minibody (referred to as the 2B3 minibody) is derived from the intact hu1G8 antibody. The 2B3 minibody was labeled with ^{131}I for tumor targeting studies and ^{124}I for microPET evaluation in four different PSCA-expressing tumor models. The 2B3 minibody showed fast blood clearance kinetics relative to the intact hu1G8 monoclonal antibody, resulting in the ability to discern clear images of prostate cancer xenografts at 21 hours versus 168 hours. Moreover, the 2B3 minibody mimicked the tumor uptake of the intact hu1G8 monoclonal antibody in the LAPC-9 model despite its rapid elimination from the circulation. Finally, the ability of the 2B3 minibody to image androgen-independent (AI) xenografts as clearly as the androgen-dependent (AD) xenografts makes it a potential rapid imaging agent for prostate cancer patients stratified into high-risk categories.

Materials and Methods

Design and gene assembly of anti-PSCA minibody. The V genes from hu1G8 (17) were individually amplified by reverse transcription-PCR (RT-PCR) and used in the assembly of a minibody gene consisting of a light chain leader sequence, a scFv fragment in the V_L-V_H orientation connected by an 18 amino acid GlySer-rich linker followed by indirect fusion to the human IgG1 C_H3 domain via the human IgG1 upper and middle hinge and a lower GlySer-linker peptide of 10 residues (23). The 2B3 minibody gene was then transferred into the pEE12 mammalian expression vector as described (22).

Cell lines. NS0 mouse myeloma (25) and the human prostate cancer cell lines PC-3 [American Type Culture Collection (ATTC)], PC-3-PSCA, and LNCaP (ATCC) transfected cells (LNCaP-PSCA) were maintained as described (17). The human B-cell lymphoma cell line SKW 6.4 (ATCC) transfected with PSCA (SKW 6.4-PSCA) was maintained as recommended, supplemented with 1% β-mercaptoethanol (1,000×; Life Technologies).

Expression, screening, propagation, and purification. The 2B3 minibody expression vector was transfected into NS0 cells as described (22). After 2 wk of selection in glutamine-deficient media, supernatants from individual cell clones were screened for 2B3 minibody expression by ELISA and Western blots as previously described (22). High-expressing clones were expanded to terminal cultures, and the level of 2B3 minibody expression was assayed by ELISA using serial dilutions of harvested supernatants with reference minibody of known concentration as a standard.

Cell culture supernatants containing the 2B3 minibody were prepared as described (26) and concentrated down to 100 mL using a Labscale TFF system concentrator (Millipore) before being dialyzed against 50 mmol/L acetic acid (pH 5). Dialyzed supernatant was then loaded onto a 1.6 mL POROS 20HS (Applied Biosystems) cation exchange chromatography column. Bound proteins were eluted with a NaCl step gradient ranging from 0 to 0.2 mol/L in 50 mmol/L acetic acid (pH 5) over 25 column volumes. Elution was monitored by UV absorption (280 nm). Eluted fractions containing the desired 2B3 minibody were pooled and diluted 5-fold with 50 mmol/L MES (pH 6.5), and reloaded onto the reequilibrated 1.6 mL cation exchange column. Bound proteins were eluted with a NaCl gradient from 0 to 0.25 mol/L in 50 mmol/L MES (pH 6.5) over 30 column volumes. The 2B3 minibody-containing fractions were pooled and dialyzed against PBS with a porous membrane tubing (molecular weight cutoff, 30,000; Spectrum Laboratories) and concentrated with a Vivaspin 20 (molecular weight cutoff, 30,000; Vivascience). The concentration and total amount of protein obtained after purification were determined by ELISA and by UV absorbance at 280 nm using an extinction coefficient (ε) of 1.4 mg/mL.

Minibody size characterization. Purified protein was analyzed by SDS-PAGE as described (22). Native size was determined by running 25 to 50 μg of purified protein isocratically in PBS on a size exclusion column (Superdex 75; GE Healthcare) using a known 80-kDa minibody as standard.

The PSCA-binding activity of the 2B3 minibody was determined by competition ELISA as described (17). Determination of relative affinity was calculated by linear extrapolation of percentage bound versus 1/nmol/L of murine 1G8, hu1G8, and the 2B3 minibody. At 50% bound, relative affinities were calculated.

Cellular PSCA-binding activity was assessed by flow cytometry. Briefly, 5×10^5 LNCaP and LNCaP-PSCA cells resuspended in 100 μL PBS/1% fetal bovine serum were incubated on ice with 10 μL 2B3 minibody (0.1 μg/μL), washed, and incubated with phycoerythrin-conjugated $F(ab')_2$ fragment (human IgG specific; Jackson ImmunoResearch). Cells were washed, pelleted, and resuspended in 0.5 mL PBS/1% fetal bovine serum, and binding data were acquired on a FACScan (BD Biosciences) and analyzed by using CellQuest software (BD Biosciences).

Radioiodination. Radioiodination with the positron emitting isotope ^{124}I (Advanced Nuclide Technologies) and labeling efficiency were determined as described (20). Immunoreactivity was determined by incubating the radioiodinated 2B3 minibody (~100,000 cpm) with SKW 6.4-PSCA cells in PBS/1% fetal bovine serum for 1 h at room temperature. Cells were pelleted and activity in an aliquot of the supernatant was counted in a Wizard 3″ 1480 Automatic Gamma Counter (Perkin-Elmer). A negative standard consisting of an equal amount of radiolabeled 2B3 minibody in PBS/1% fetal bovine serum without cells was used as a total activity reference. The decrease in radionuclide activity relative to the standard determined the immunoreactivity (20).

^{124}I microPET imaging and biodistribution. All animal handling was done under a protocol approved by the Chancellor's Animal Research Committee of the University of California in Los Angeles (UCLA). PC-3 (antigen negative) and LAPC-9 (antigen positive) xenografts were established as described (17). In another model, 2×10^6 PC-3 and PC-3-PSCA cells were injected in the left and right shoulders of 6-wk-old female athymic mice, respectively. LAPC-9 AI xenografts were established in castrated 6-wk-old male mice as described (27). PC-3 tumors were allowed to grow for 2 wk, whereas LAPC-9 tumors were allowed to grow for 4 wk. Thyroid and stomach uptake of radioiodine was blocked as described (21).

For the PC-3 and LAPC-9 (AD and AI) models, the mice (n = 16; four experimental sets of four mice) were each injected with ~50 μg of ^{124}I-hu 2B3 minibody (specific activity of 1.8 ± 0.7 μCi/μg) in saline/1% human serum albumin (Sigma-Aldrich) via the tail vein. In the irrelevant minibody experiment, 50 μg of ^{124}I-labeled protein (specific activity of 1.5 μCi/μg) was also injected in LAPC-9 AD–bearing mice (n = 4). At 4 and 21 h postinjection, the mice were anesthetized using 2% isoflurane, and imaged with a Focus microPET scanner (Concorde Microsystems Inc.) as previously described (26). Acquisition time was 10 min (1 bed position), and images were reconstructed using a filtered back projection reconstruction algorithm (28) and displayed using the AMIDE software package (29). At the late time point, selected mice were also imaged by micro computed tomography (microCT), and the images were coregistered with the microPET scans for anatomic reference and accuracy (30). Coronal projections were used to show the activity of the entire mouse at each given time point. Images were normalized for an individual mouse at different time points within the same experiment but not across different experiments.

The mice were euthanized following the 21-h scan. Tumors, liver, kidneys, lung, spleen, and carcass were harvested, weighed, and γ counted. Radioactive uptake in organs was corrected for radioactive decay and converted to percentage of injected dose per gram (% ID/g) tissue.

Tumor targeting and pharmacokinetic biodistribution of ^{131}I-2B3-minibody in severe combined immunodeficiency mice. Six-week-old male severe combined immunodeficient (SCID) mice (n = 4) were injected s.c. into the right shoulder region with 3×10^6 LNCaP-PSCA cells. Thirty days post cell injection, three mice were each injected with 8.5 μg (specific activity = 0.6 μCi/μg) of ^{131}I-2B3 minibody via the tail vein. At 21 h postinjection, the mice were sacrificed and major organs were dissected, weighed, and counted.

For biodistribution studies in non–tumor-bearing mice, SCID mice (n = 18) were each injected with 11 μg (specific activity = 1.11 μCi/μg) of ^{131}I-labeled 2B3 minibody via the tail vein. Groups of three mice were euthanized at 0, 2, 6, 12, 24, and 48 h postinjection. Major organs and blood were harvested, weighed, and counted. The blood clearance curve was calculated using a biexponential fit with the UCLA Kinetic Imaging System (31).

MicroPET data analysis. Cylindrical regions of interest (ROI) were drawn from three-dimensional filtered back projection reconstructed PET images, coregistered with CT, at 4 and 21 h using AMIDE (29). In the sagittal orientation, four ROIs were drawn per tumor as well as in areas outside the animal termed "scatter." In the coronal orientation, four ROIs were drawn over the low-activity triceps muscle area adjacent to the tumors and termed "background." The mean scatter-ROI values were subtracted from the tumor and background (muscle) ROI values, before calculation of tumor-to-background ratios. The positive tumor-to-negative tumor ratios were also determined after subtracting background scatter-ROI values. Statistical analysis was done using Excel 2000 (Microsoft). Student's t test with a 1-tailed distribution and 2-sample unequal variance parameter was used to assess the significance between tumor activity and background activity. All significance testing was determined at the $P < 0.01$ level.

Results

Biochemical characterization of 2B3 minibody. Engineered 2B3 minibody was successfully expressed and yielded levels of ~20 mg/L in terminal culture (~300 mL batches). Analysis of purified 2B3 minibody by SDS-PAGE (Fig. 1A) showed that under reducing conditions, the minibody migrated as a monomer consistent with its predicted molecular weight of ~40 kDa (*lane 2*) and as a covalent dimer of ~80 kDa under nonreducing conditions (*lane 1*). Size exclusion chromatography verified that the 2B3 minibody eluted as a uniform peak at a time (~29 minutes) corresponding to a correctly folded dimer of expected molecular weight (Fig. 1B) similar to a reference minibody (not shown).

Functional characterization of 2B3 minibody. Following 2B3 minibody production, PSCA recognition and binding were evaluated. Flow cytometry (Fig. 1C) showed that the 2B3 minibody could discriminate LNCaP-PSCA cells. Clear differential staining is evident for the 2B3 minibody on PSCA-positive LNCaP cells and not on PSCA-negative LNCaP cells. The secondary antibody used for detecting the 2B3 minibody did not bind to either LNCaP or LNCaP-PSCA cells.

The affinity of the 2B3 minibody was evaluated by binding to recombinant soluble PSCA. Previously, the intact mouse 1G8 and hu1G8 antibodies were estimated to have an apparent K_D of 2.6 and 16.7 nmol/L.[3] In the competition ELISA done in this study, the relative affinities of intact 1G8 antibody, hu1G8 antibody, and 2B3 minibody were 5 nmol/L, 25 nmol/L, and 46 nmol/L, respectively (Fig. 1D). This represents a ~9-fold loss in relative affinity to the mouse 1G8 antibody and a ~2-fold relative loss to hu1G8 antibody for the engineered minibody fragment.

Binding to PSCA was also evaluated following radioiodination of the 2B3 minibody using SKW 6.4-PSCA cells. The

[3] E. Lepin, J.V. Leyton, Y. Zhou, T. Olafsen, J.D. Marks, A.M. Wu, unpublished data.

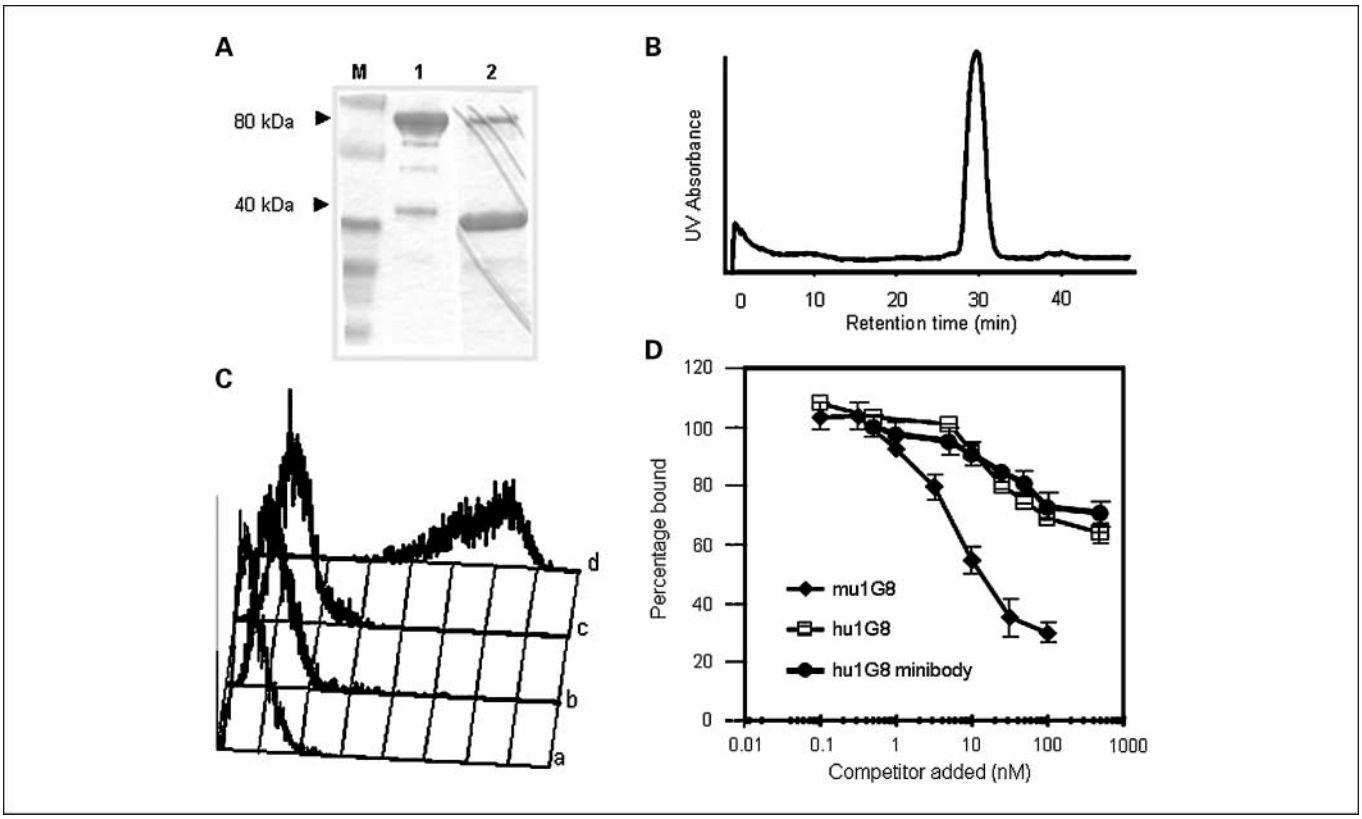

Fig. 1. *A,* SDS-PAGE analysis of anti-PSCA 2B3 minibody under nonreducing (*lane 1*) and reducing (*lane 2*) conditions. M, molecular weight markers. *B,* size exclusion chromatography profile of purified 2B3 minibody on a calibrated Superdex 75 column. *C,* flow cytometry (*a*) LNCaP and (*c*) LNCaP-PSCA cells incubated with secondary antihuman (Fc-specific) phycoerythrin-F(ab')$_2$ only or (*b*) LNCaP or (*d*) LNCAP-PSCA cells incubated with purified 2B3 minibody (0.1 μg/μL). *D,* competition ELISA binding assay against recombinant PSCA.

immunoreactivity of the 2B3 minibody was 32% (±13; n = 5) following radioiodination with ^{124}I. The immunoreactivity following two separate labeling reactions with ^{131}I was 40 and 30%.

MicroPET imaging of LAPC-9 xenografts using ^{124}I-2B3 minibody. MicroPET imaging was used to evaluate the *in vivo* tumor-targeting ability of the 2B3 minibody. For this purpose, the LAPC-9 model was selected as the target xenograft for its high level of endogenous PSCA expression (11). MicroPET images at 4 hours of male SCID mice (n = 4) bearing xenografts of 218 mg (±190) revealed the ability of the ^{124}I-2B3 minibody to discern the xenograft suggesting rapid tumor localization (Fig. 2A). In addition, circulating activity in the thorax, abdomen, and bladder was prominent. At 21 hours, increased signal is seen in the tumor with reduced circulating activity in the thorax, abdomen, and bladder resulting in enhanced contrast tumor image (Fig. 2B). The microPET/microCT overlay projection verifies the anatomic location of the tumor (Fig. 2C). The ^{124}I-2B3 minibody exhibited similar biodistribution when evaluated by PET imaging in a set of larger LAPC-9 tumors of 1.8 g (±0.6; n = 4). At 4 hours, specific signal is seen in the tumor (Fig. 2D). Again, nonspecific signal is present in the thorax, abdomen, and bladder. At 21 hours, the activity in the tumor is stronger with diminished activity in the nonspecific areas (Fig. 2E). The microPET/microCT overlay again shows signal coming from the xenograft (Fig. 2F).

The biodistribution at 21 hours for the mouse in Fig. 2A to C revealed that the tumor uptake reached 7.1% ID/g, whereas the blood, liver, spleen, lung, and kidney each had uptakes of 4.7, 1.2, 1.3, 3.4, and 1.7% ID/g, respectively. The average tumor uptake in the group was 4.7% ID/g. Table 1 summarizes the collected uptakes of all the LAPC-9 tumors (n = 12), and other tissues of interest.

2B3 minibody PSCA-xenograft specificity. To evaluate whether the targeting of the 2B3 minibody was specific *in vivo*, a double tumor model was established with antigen-positive (LAPC-9) and antigen-negative (PC-3) prostate cancer xenografts (Fig. 3A and B). The average tumor weight in four mice was 759 (±419) and 298 (±34) mg for the LAPC-9 and PC-3 xenografts, respectively. Figure 3A shows strong activity accumulation in the PSCA-positive LAPC-9 tumor and minimal uptake in the PSCA-negative xenograft at 21 hours. Figure 3B shows the microPET/microCT overlay for anatomic confirmation of the tumors. The average uptake in LAPC-9 for this set of mice was 5.5% ID/g (±0.7), which was significantly higher (P < 0.01) than the nonspecific tumor uptake in the PC-3 xenografts of 2.9% ID/g (±0.3). The liver, spleen, lung, and kidney uptakes were 2.0, 2.2, 4.1, and 2.8% ID/g, respectively. The biodistribution at 21 hours was consistent with the biodistribution seen with the single LAPC-9 tumor–bearing mice and is therefore incorporated into Table 1.

To further evaluate specificity, an irrelevant minibody fragment was labeled with ^{124}I and assessed in mice bearing

LAPC-9 xenografts [tumor size of 292 mg (±98)]. As seen in Fig. 3C, the microPET/microCT image at 21 hours shows that the control minibody does not localize to the xenograft. Biodistribution at the time of sacrifice (28 hours) revealed a tumor uptake of 0.6% ID/g (±0.2; n = 4). Thus, the uptake seen with the 2B3 minibody in the LAPC-9 xenografts is specific and not due to nonspecific tumor accumulation.

Minibody blood kinetics in non–tumor-bearing SCID mice. To evaluate kinetics of distribution in the absence of tumor, the 2B3 minibody was radiolabeled with ^{131}I, and biodistribution and blood clearance studies were conducted in SCID mice. The ^{131}I-2B3 minibody showed a somewhat prolonged blood clearance pattern relative to that seen with other minibody fragments targeting carcinoembryonic antigen and HER2 ($t_{1/2}\beta$ = 7.0 and 5.6 hours, respectively; refs. 22, 24). For the ^{131}I-2B3 minibody, the distribution phase half-life ($t_{1/2}\alpha$) was 1.3 hours and the terminal phase half-life ($t_{1/2}\beta$) was 11.2 hours (Fig. 4). The liver, spleen, and kidneys displayed low nonspecific uptake that fell below 1% ID/g by 24 hours, which is consistent with that observed for other minibody fragments. The blood activity was 2.4% ID/g at 24 hours.

Targeting of LNCaP-PSCA xenografts using ^{131}I-2B3 minibody. Many targeting studies for prostate cancer have been conducted with LNCaP xenografts. Therefore, using SCID mice bearing generated LNCaP-PSCA tumors, a 21-hour time point biodistribution and tumor uptake of the ^{131}I-labeled 2B3 minibody was evaluated. At 21 hours, high activity was present in the tumor with low blood and organ activity (Table 1). Tumor uptake was 9.3% ID/g (±2.3), whereas the blood was 3.3% ID/g (±1.6), resulting in a tumor-to-blood ratio of 2.8.

MicroPET imaging of AI xenografts using ^{124}I-2B3 minibody. Targeting and imaging of AI xenografts was also explored in two separate experiments. The PC-3 cell line was engineered to stably express PSCA (16); thus, an imaging study could be undertaken with a negative cell line that is a matched control. In this dual tumor model, ^{124}I-2B3 minibody accumulation is clearly seen favoring the PSCA-positive (right shoulder) tumor at 21 hours (Fig. 5A). LAPC-9 AI xenografts have also been developed, and PET imaging of the ^{124}I-2B3 minibody in LAPC-9 AI tumor–bearing mice is depicted in Fig. 5B. As seen with the LAPC-9 AD xenografts, the localization of the activity is in the tumor with minimal nonspecific activity in the midsection and typical bladder activity.

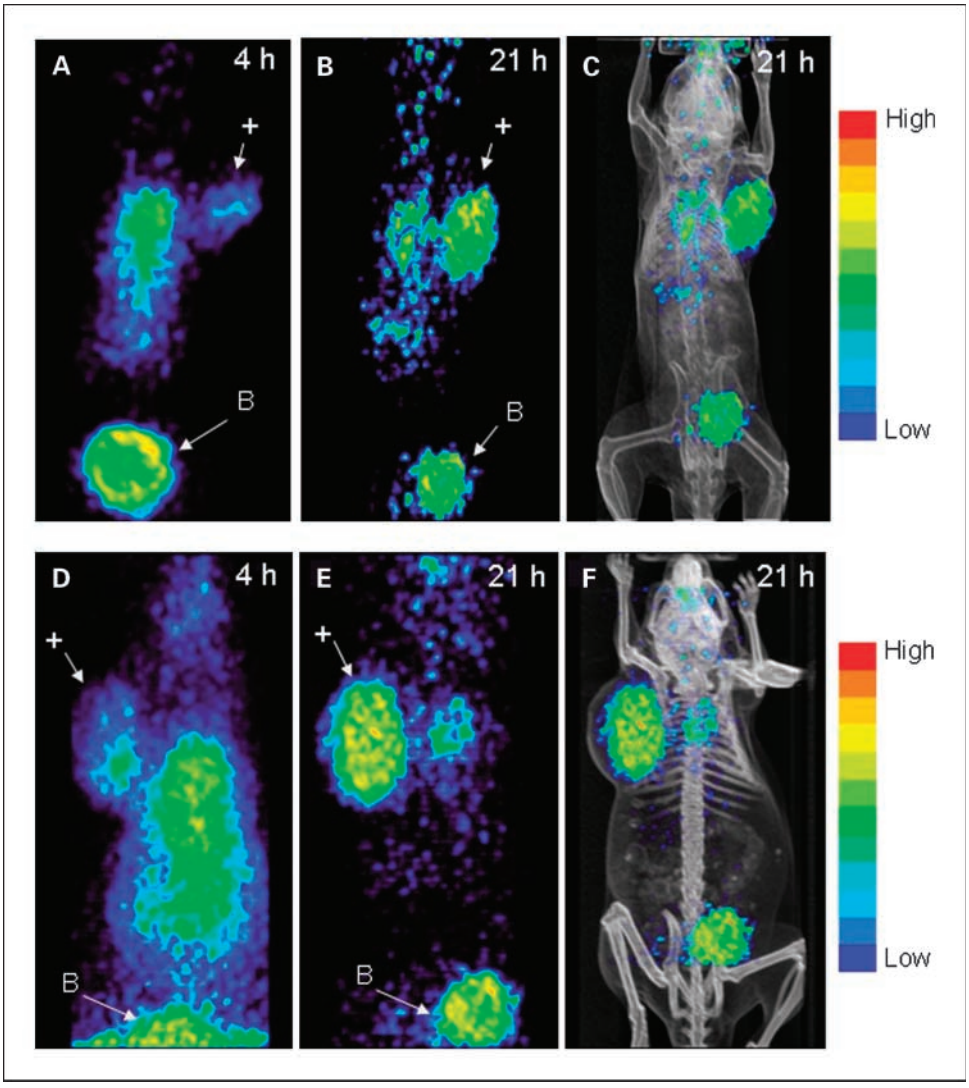

Fig. 2. Coronal microPET projections of mouse bearing an LAPC-9 xenograft of (*A-C*) 251 mg (+ *arrow*) and (*D-F*) 1.8 g (+ *arrow*). Mice were injected with ^{124}I-2B3 minibody (~50 μg/mouse) and serially imaged at 4 h (*A* and *D*) and 21 h (*B* and *E*). MicroPET/microCT projection overlay at 21 h is shown in *C* and *F*. The images are scaled to the same threshold. Color scale indicated. B, bladder.

Table 1. Biodistribution of radioiodinated-2B3 minibody in different PSCA-positive tumor bearing mice at 21 h postinjection

Tissue	LAPC-9 ^{124}I (n = 12)	LNCaP-PSCA ^{131}I (n = 4)	PC-3-PSCA ^{124}I (n = 4)	LAPC-9 AI ^{124}I (n = 4)
Positive tumor (T)	5.2 ± 1.6	9.3 ± 2.3	2.4 ± 0.2	2.5 ± 1.0
Negative tumor (PC-3)	2.6 ± 0.2*†	ND	0.7 ± 0.3‡	ND
Liver	1.3 ± 0.3†	1.1 ± 0.3§	0.5 ± 0.1‡	0.9 ± 0.2
Spleen	1.5 ± 0.5†	0.7 ± 0.4§	0.6 ± 0.2‡	0.8 ± 0.1
Kidney	1.9 ± 0.5†	2.0 ± 0.4§	0.8 ± 0.2‡	1.3 ± 0.2
Lung	3.4 ± 1.0†	2.1 ± 0.3§	1.2 ± 0.5	2.1 ± 0.4
Blood	4.9 ± 1.3	3.3 ± 1.6§	2.3 ± 0.6	3.4 ± 0.5
Carcass	1.2 ± 0.1†‖	ND	ND	0.6 ± 0.2
Ratios				
T/blood	1.1	2.8	1.0	0.7
T/liver	4.0	8.5	4.8	2.8
T/kidney	2.7	4.7	3.0	1.9
T/neg tumor	2.0	ND	3.4	ND
Tumor weight (mg)				
PSCA-positive	910 ± 740	160 ± 40	150 ± 60	1,640 ± 210
PC-3	300 ± 130	ND	181 ± 64	ND

NOTE: Numbers represent mean uptake expressed in %ID/g ± SD.
Abbreviation: ND, not determined.
*n = 4.
†Significantly different from LAPC-9 uptake (P < 0.01).
‡Significantly different from PC-3-PSCA uptake (P < 0.01).
§Significantly different from LNCaP-PSCA uptake (P < 0.01).
‖n = 8.

Biodistribution of excised AI tumors showed moderate uptake compared with the AD xenografts (Table 1). Uptake in the PC-3-PSCA positive tumor was 2.4% ID/g (±0.2), which was significantly higher (P < 0.01) at 21 hours than the uptake in the PC-3 tumor at 0.7% ID/g (±0.3), resulting in a 3.4 positive-to-negative tumor ratio. This study shows specific PSCA-targeting in an AI tumor model. Activities in the liver, spleen, kidney, and lung were at low levels.

ROI data analysis. In the LAPC-9 AD xenograft model, ROI analysis at the early 4-hour time point resulted in a tumor-to-background ratio of 1.3. At the later 21-hour time point the contrast ratio improved to 5.3 resulting in a 4.1-fold improvement. In the LAPC-9 AI model, a tumor-to-background ratio of 3.3 was obtained at 21 hours. For the PC-3-PSCA model, the tumor-to-background ratio was 0.7 at 4 hours, which improved to 3.7 at 21 hours, resulting in a 5.3-fold improvement.

ROI analysis was also carried out to determine the ratio of PSCA positive-to-negative xenografts. In the LAPC-9 AD model, the LAPC-9-to-PC-3 ratio was 2 at 21 hours. In the AI model with a matched PSCA-positive xenograft; the PC-3-PSCA-to-PC-3 ratio was also 2 at 21 hours.

Discussion

The present study introduces the genetically engineered radioiodinated (^{124}I or ^{131}I) 2B3 minibody as a novel antibody fragment for specific targeting and potential PET imaging agent for PSCA-expressing prostate cancers. The 2B3 minibody was evaluated by microPET in mice with different PSCA-expressing

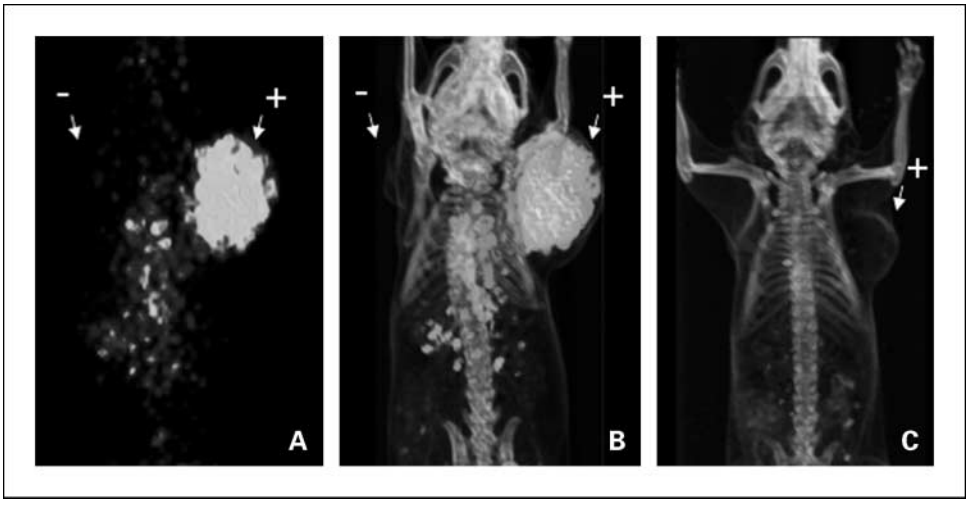

Fig. 3. Coronal microPET (*A*) and microPET/microCT (*B*) overlay projections of a SCID mouse bearing LAPC-9 (+ *arrow*) and PC-3 (- *arrow*) xenografts at 21 h injected with ^{124}I-2B3. *C,* coronal microPET/microCT overlay projection of LAPC-9 (+)-bearing mouse at 21 h injected with irrelevant ^{124}I-labeled minibody (~50 μg). Mouse in *A* and *B* not scaled to mouse in *C*.

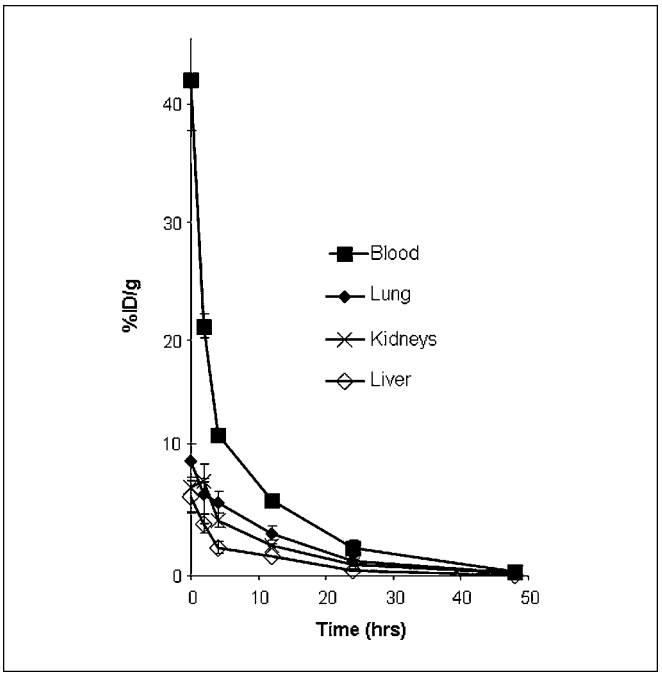

Fig. 4. Biodistribution of ^{131}I-2B3 minibody in non – tumor-bearing male SCID mice. Groups of three mice were evaluated at each time point.

prostate cancer xenografts. Rapid uptake was noted by the ability to visually discriminate the various xenografts at 4 hours whereas rapid blood clearance showed the ability to produce enhanced-contrast images at 21 hours. Biochemical analysis showed that the minibody was pure following chromatography, migrated as a covalent dimer, had high affinity, and could discriminate PSCA *in vitro*. Furthermore, the ^{124}I-2B3 minibody was able to image and target PSCA-positive AI xenografts, revealing that AI as well as AD tumors could be targeted. Pharmacokinetic studies showed a rapid yet slightly longer half-life compared with other tumor-targeting minibody fragments. Nonetheless, the 2B3 minibody clearance proved rapid enough to provide high-contrast images by 21 hours. ROI determination of tumor-to-background ratios at different time points showed improved tumor-to-background ratios from 4 to 21 hours. Importantly, *in vivo* specificity was shown by minimal uptake in the PSCA-negative tumors and lack of tumor targeting by an irrelevant minibody. Thus, the 2B3 minibody displayed multiple positive xenograft targeting characteristics *in vivo*, proving itself as a promising candidate for imaging prostate cancer.

The present 80-kDa anti-PSCA minibody fragment was derived from the hu1G8 monoclonal antibody, which has a high relative affinity (K_D = 25 nmol/L) for PSCA (17). The hu1G8 monoclonal antibody was humanized from the mouse monoclonal 1G8 antibody (K_D = 1 nmol/L; ref. 16). The ^{124}I-labeled intact murine 1G8 and hu1G8 monoclonal antibodies were shown to successfully image PSCA-positive LAPC-9 xenografts in male SCID mice (17), reaching good tumor uptakes. However, a long delay was necessary to produce enhanced-contrast tumor images. At times as late as 72 hours, high activity remained in the blood and normal tissue, making tumor identification more difficult. In the current work, the smaller minibody tracer mimicked the large intact antibodies in LAPC-9 uptake, but reduced the time needed for optimal PET imaging to 21 hours rather than 168 hours. The LAPC-9 xenograft is one of the few available tumors that endogenously overexpress PSCA. This xenograft line was established from a patient with metastatic prostate cancer (32) and has been a benchmark for PSCA expression evaluation experiments (11, 12). In this model, the ^{124}I-2B3 minibody showed similar tumor uptake (5.2% ID/g) at 21 hours to that of the ^{124}I-labeled murine 1G8 (5.8% ID/g) and hu1G8 (6.6% ID/g) monoclonal antibodies at 168 hours (17).

The LNCaP cell line of human prostate cancer has commonly been used for investigating antibody imaging and therapeutic approaches for prostate cancer (9, 33, 34). In the LNCaP-PSCA model, high tumor uptake (9.3% ID/g) with the ^{131}I-2B3 minibody was achieved as well as a higher tumor-to-blood ratio (2.8) than that seen in the LAPC-9 model. Recently, we have

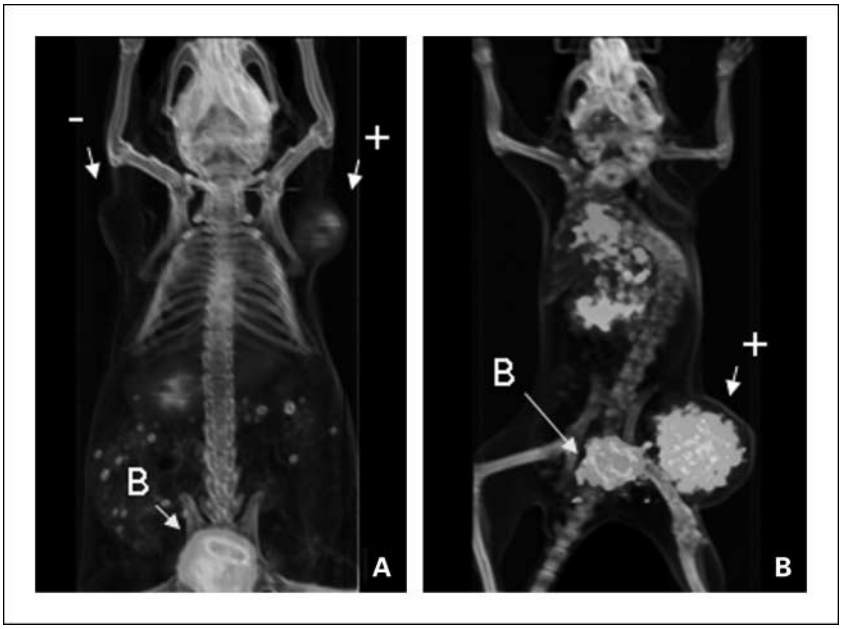

Fig. 5. *A,* coronal microPET/CT projections of a representative athymic mouse bearing PC-3-PSCA (+ *arrow*) and PC-3 (- *arrow*) xenografts and (*B*) a SCID mouse bearing a LAPC-9 AI xenograft (+ *arrow*) injected with ^{124}I-2B3 minibody at 21 h. B, bladder.

determined that the LNCaP-PSCA xenograft expresses PSCA at much higher levels than the LAPC-9 xenograft,[4] suggesting a possible correlation between tumor uptake and antigen abundance. It will be of interest to formally evaluate the ability of the 2B3 minibody to image xenografts of various PSCA antigen expression levels, given the known heterogeneous nature of prostate cancer.

Patients with prostate cancer die from metastatic hormone refractory disease (35). Although the role of PSCA in progression to androgen independence is still under investigation, PSCA expression has been shown to be up-regulated in a majority of prostate cancer metastases (12) and overexpressed in 83% of AI specimens (11). Therefore, we asked whether the 2B3 minibody could be used to detect hormone refractory tumors in our xenograft model. In response to castration, LAPC-9 cells undergo growth arrest and persist in a dormant, androgen-responsive state for at least 6 months. After prolonged periods of androgen deprivation, spontaneous AI outgrowths develop (27). Using this xenograft model, the ^{124}I-2B3 minibody showed the ability to target and produce high-contrast tumor images at 21 hours. In addition, the ^{124}I-2B3 minibody was able to image PC3-PSCA-expressing xenografts. These animals contained PSCA-negative PC-3 xenografts that allowed evaluation of nonspecific tumor uptake. The PSCA positive-to-negative tumor ratio was 3.4, displaying clear evidence of PSCA specificity in this AI model.

The most extensively evaluated nuclear imaging agent for prostate cancer is Prostascint, which recognizes prostate-specific membrane antigen. In preclinical studies, the radioiodinated parental antibody of Prostascint (7E11) was compared head-to-head with another radioiodinated anti–prostate-specific membrane antigen antibody (J591) for its tumor-targeting potential in LNCaP xenografts (36). In a biodistribution study (tumor size range, 100-300 mg), the tumor uptake was 11.7% ID/g (±4.3) and 11.2% ID/g (±2.9) for 7E11 and J591, respectively, at 48 hours. The blood activity, however, was 10.8% ID/g (±3.5) for 7E11 and 8.6% ID/g (±2.0) for J591, resulting in a tumor-to-blood ratio of 1 which only rose to 2 by 144 hours (34). In this work, uptake in LNCaP-PSCA tumors with the radioiodinated 2B3 minibody reached 9.3% ID/g (±2.3) at 21 hours and the tumor-to-blood ratio was nearly 3. Thus, in the same xenograft model, the 2B3 minibody reached a comparable tumor uptake level with an improved tumor-to-blood ratio at 21 hours, instead of 144 hours. Protease-derived ^{125}I-J591 F(ab′)$_2$ (110 kDa) and Fab (50 kDa) fragments were also evaluated for their ability to improve target-to-background ratios in LNCaP xenografts (37). The tumor and blood activity for ^{125}I-J591 F(ab′)$_2$ were 5.17 and 4.41% ID/g, respectively, at 24 hours. The tumor uptake with the ^{125}I-J591 Fab reached a modest 1.85% ID/g at 24 hours but importantly a tumor-to-blood ratio of 3.44 was achieved (37). This study showed that antibody fragments improved target-to-background ratios at an earlier time point than intact IgG.

Tumor targeting of cell surface antigens by using small peptides has also become a focus of interest due to the favorable properties of peptides. High receptor affinity and very fast blood clearance allows peptides to achieve high target-to-background ratios very early after administration injection (reviewed in ref. 38). Two recent PET imaging studies using peptides labeled with the positron emitter ^{64}Cu ($t_{1/2}$ = 12.7 hours) have shown promise as prostate cancer imaging agents (39, 40). In one study, the stability and pharmacokinetics of ^{64}Cu-bombesin (BBN) peptide using either CB-TE2A or DOTA as metal chelators were compared in mice bearing PC-3 xenografts (39). The ^{64}Cu- CB-TE2A-bombesin peptide exhibited better tumor targeting at 15 minutes after administration as well as improved *in vivo* stability that resulted in substantial decrease in liver uptake and improved clearance from the mouse at 24 hours. In a more recent study, a vasoactive intestinal peptide analogue (TP3939) targeting the VPAC1 receptor, radiolabeled with ^{64}Cu was evaluated in mice carrying PC3 xenografts (40). MicroPET images at 4 and 24 hours showed specific localization to tumors with tumor to muscle and tumor to blood ratios of 5.2 and 2.5, respectively, at 24 hours. The ^{64}Cu-TP3939 also showed the ability to detect occult prostate cancer in the mouse prostate in the natural TRAMP II model of prostate cancer development that was not detected by ^{18}F-FDG.

The current study shows the combination of the high sensitivity and resolution of PET with the high specificity, selectivity, and the suitable pharmacokinetics of the 2B3 minibody. An important next step will be an evaluation of radioiodinated 2B3 minibody in pilot imaging studies in patients with known metastatic prostate cancer, to evaluate normal tissue distribution, pharmacokinetics, and tumor localization, and to assess immunologic responses, if any. In addition, the studies reported here have been undertaken exclusively with radioiodine, and it will be important to evaluate radiometal-labeled 2B3 minibody uptake and imaging in these same xenograft models. PET imaging using ^{64}Cu could be an advantage because there is evidence of antibody internalization with PSCA (41) and the ^{64}Cu-labeled minibody showed excellent tumor images in a different internalizing system (42).

In patients, by the time of diagnosis, only half of the tumors are clinically localized whereas the other half have detectable or undetectable extracapsular spread in patients with prostate cancer (43). Antibody-based PET (immunoPET) detection of PSCA provides a biological basis of imaging based on a tissue-specific marker, which would complement current anatomic and metabolic approaches to detection and monitoring of disease. As such, immunoPET could play an important role in staging at diagnosis, stratifying patients for PSCA-targeted therapies, monitoring treatment response, and in long-term follow-up. Future development of the ^{124}I-labeled anti-PSCA 2B3 minibody for clinical PET imaging will provide an important new modality for detection and management of prostate cancer.

Disclosure of Potential Conflicts of Interest

No potential conflicts of interest were disclosed.

Acknowledgments

We thank Dr. D. Stout, J. Edwards, and W. Ladno at UCLA for their assistance with the microPET/CT scans; F.B. Salazar for providing excellent technical assistance; Dr. V.E. Kenanova for providing help with image analysis; Drs. Z. Gu and J. Yamashiro for critical analysis of data; Dr. H. Huang for assistance with kinetic analysis; and the UCLA Jonsson Comprehensive Cancer Center and Center for AIDS Research Flow Cytometry Core Facility.

[4] Unpublished data.

References

1. Bouchelouche K, Oehr P. Positron emission tomography and positron emission tomography/computerized tomography of urological malignancies: an update review. J Urol 2008;179:34–45.
2. Takahashi N, Inoue T, Lee J, Yamaguchi T, Shizukuishi K. The roles of PET and PET/CT in the diagnosis and management of prostate cancer. Oncology 2007;72: 226–33.
3. Pucar D, Sella T, Schoder H. The role of imaging in the detection of prostate cancer local recurrence after radiation therapy and surgery. Curr Opin Urol 2008; 18:87–97.
4. Vavere AL, Kridel SJ, Wheeler FB, Lewis JS. 1-11C-acetate as a PET radiopharmaceutical for imaging fatty acid synthase expression in prostate cancer. J Nucl Med 2008;49:327–34.
5. Schoder H, Larson SM. Positron emission tomography for prostate, bladder, and renal cancer. Semin Nucl Med 2004;34:274–92.
6. Schuster DM, Votaw JR, Nieh PT, et al. Initial experience with the radiotracer anti-1-amino-3-18F-fluorocyclobutane-1-carboxylic acid with PET/CT in prostate carcinoma. J Nucl Med 2007;48:56–63.
7. Mohammed AA, Shergill IS, Vandal MT, Gujral SS. ProstaScint and its role in the diagnosis of prostate cancer. Expert Rev Mol Diagn 2007;7:345–9.
8. Brassell SA, Rosner IL, McLeod DG. Update on magnetic resonance imaging, ProstaScint, and novel imaging in prostate cancer. Curr Opin Urol 2005;15: 163–6.
9. Barren RJ III, Holmes EH, Boynton AL, Misrock SL, Murphy GP. Monoclonal antibody 7E11.C5 staining of viable LNCaP cells. Prostate 1997;30:65–8.
10. Reiter RE, Gu Z, Watabe T, et al. Prostate stem cell antigen: a cell surface marker overexpressed in prostate cancer. Proc Natl Acad Sci U S A 1998;95: 1735–40.
11. Gu Z, Thomas G, Yamashiro J, et al. Prostate stem cell antigen (PSCA) expression increases with high Gleason score, advanced stage and bone metastasis in prostate cancer. Oncogene 2000;19:1288–96.
12. Lam JS, Yamashiro J, Shintaku IP, et al. Prostate stem cell antigen is overexpressed in prostate cancer metastases. Clin Cancer Res 2005;11:2591–6.
13. Amara N, Palapattu GS, Schrage M, et al. Prostate stem cell antigen is overexpressed in human transitional cell carcinoma. Cancer Res 2001;61:4660–5.
14. Argani P, Rosty C, Reiter RE, et al. Discovery of new markers of cancer through serial analysis of gene expression: prostate stem cell antigen is overexpressed in pancreatic adenocarcinoma. Cancer Res 2001;61: 4320–4.
15. McCarthy DM, Maitra A, Argani P, et al. Novel markers of pancreatic adenocarcinoma in fine-needle aspiration: mesothelin and prostate stem cell antigen labeling increases accuracy in cytologically borderline cases. Appl Immunohistochem Mol Morphol 2003;11: 238–43.
16. Saffran DC, Raitano AB, Hubert RS, Witte ON, Reiter RE, Jakobovits A. Anti-PSCA mAbs inhibit tumor growth and metastasis formation and prolong the survival of mice bearing human prostate cancer xenografts. Proc Natl Acad Sci U S A 2001;98: 2658–63.
17. Olafsen T, Gu Z, Sherman MA, et al. Targeting, imaging, and therapy using a humanized antiprostate stem cell antigen (PSCA) antibody. J Immunother 2007;30: 396–405.
18. Wu AM, Senter PD. Arming antibodies: prospects and challenges for immunoconjugates. Nat Biotechnol 2005;23:1137–46.
19. Wu AM, Yazaki PJ. Designer genes: recombinant antibody fragments for biological imaging. Q J Nucl Med 2000;44:268–83.
20. Olafsen T, Kenanova VE, Wu AM. Tunable pharmacokinetics: modifying the *in vivo* half-life of antibodies by directed mutagenesis of the Fc fragment. Nat Protoc 2006;1:2048–60.
21. Sundaresan G, Yazaki PJ, Shively JE, et al. ^{124}I-labeled engineered anti-CEA minibodies and diabodies allow high-contrast, antigen-specific small-animal PET imaging of xenografts in athymic mice. J Nucl Med 2003;44:1962–9.
22. Olafsen T, Tan GJ, Cheung CW, et al. Characterization of engineered anti-p185HER-2 (scFv-CH3)2 antibody fragments (minibodies) for tumor targeting. Protein Eng Des Sel 2004;17:315–23.
23. Hu S, Shively L, Raubitschek A, et al. Minibody: a novel engineered anti-carcinoembryonic antigen antibody fragment (single-chain Fv-CH3) which exhibits rapid, high-level targeting of xenografts. Cancer Res 1996;56:3055–61.
24. Yazaki PJ, Wu AM, Tsai SW, et al. Tumor targeting of radiometal labeled anti-CEA recombinant T84.66 diabody and t84.66 minibody: comparison to radioiodinated fragments. Bioconjug Chem 2001;12:220–8.
25. Galfre G, Milstein C. Preparation of monoclonal antibodies: strategies and procedures. Methods Enzymol 1981;73:3–46.
26. Kenanova V, Olafsen T, Crow DM, et al. Tailoring the pharmacokinetics and positron emission tomography imaging properties of anti-carcinoembryonic antigen single-chain Fv-Fc antibody fragments. Cancer Res 2005;65:622–31.
27. Craft N, Chhor C, Tran C, et al. Evidence for clonal outgrowth of androgen-independent prostate cancer cells from androgen-dependent tumors through a two-step process. Cancer Res 1999;59:5030–6.
28. Defrise M, Kinahan PE, Townsend DW, Michel C, Sibomana M, Newport DF. Exact and approximate rebinning algorithms for 3-D PET data. IEEE Trans Med Imaging 1997;16:145–58.
29. Loening AM, Gambhir SS. AMIDE: a free software tool for multimodality medical image analysis. Mol Imaging 2003;2:131–7.
30. Chow PL, Stout DB, Komisopoulou E, Chatziioannou AF. A method of image registration for small animal, multi-modality imaging. Phys Med Biol 2006;51: 379–90.
31. Huang SC, Truong D, Wu HM, et al. An internet-based "kinetic imaging system" (KIS) for MicroPET. Mol Imaging Biol 2005;7:330–41.
32. Whang YE, Wu X, Suzuki H, et al. Inactivation of the tumor suppressor PTEN/MMAC1 in advanced human prostate cancer through loss of expression. Proc Natl Acad Sci U S A 1998;95:5246–50.
33. Israeli RS, Powell CT, Corr JG, Fair WR, Heston WD. Expression of the prostate-specific membrane antigen. Cancer Res 1994;54:1807–11.
34. Smith-Jones PM, Vallabhajosula S, Navarro V, Bastidas D, Goldsmith SJ, Bander NH. Radiolabeled monoclonal antibodies specific to the extracellular domain of prostate-specific membrane antigen: preclinical studies in nude mice bearing LNCaP human prostate tumor. J Nucl Med 2003;44:610–7.
35. Jemal A, Siegel R, Ward E, Murray T, Xu J, Thun MJ. Cancer statistics, 2007. CA Cancer J Clin 2007;57: 43–66.
36. Haseman MK, Rosenthal SA, Polascik TJ. Capromab pendetide imaging of prostate cancer. Cancer Biother Radiopharm 2000;15:131–40.
37. Carter T, Sterling-Levis K, Ow K, et al. Biodistributions of intact monoclonal antibodies and fragments of BLCA-38, a new prostate cancer directed antibody. Cancer Immunol Immunother 2004;53: 533–42.
38. Aina OH, Liu R, Sutcliffe JL, Marik J, Pan CX, Lam KS. From combinatorial chemistry to cancer-targeting peptides. Mol Pharm 2007;4:631–51.
39. Garrison JC, Rold TL, Sieckman GL, et al. *In vivo* evaluation and small-animal PET/CT of a prostate cancer mouse model using 64Cu bombesin analogs: side-by-side comparison of the CB-TE2A and DOTA chelation systems. J Nucl Med 2007;48:1327–37.
40. Zhang K, Aruva MR, Shanthly N, et al. PET imaging of VPAC1 expression in experimental and spontaneous prostate cancer. J Nucl Med 2008;49:112–21.
41. Ross S, Spencer SD, Holcomb I, et al. Prostate stem cell antigen as therapy target: tissue expression and *in vivo* efficacy of an immunoconjugate. Cancer Res 2002;62:2546–53.
42. Olafsen T, Kenanova VE, Sundaresan G, et al. Optimizing radiolabeled engineered anti-p185HER2 antibody fragments for *in vivo* imaging. Cancer Res 2005;65:5907–16.
43. Kotzerke J, Gschwend JE, Neumaier B. PET for prostate cancer imaging: still a quandary or the ultimate solution? J Nucl Med 2002;43:200–2.